Applied Thermal Engineering 222 (2023) 119934

Contents lists available at ScienceDirect

Applied Thermal Engineering

journal homepage: www.elsevier.com/locate/ate

Research Paper

On the impact of turbocharger thermo-mechanical limitations on new generation gasoline engines

José Ramón Serrano, Héctor Climent, Joaquín De la Morena, Alejandro Gómez-Vilanova *

CMT-Motores Térmicos, Universitat Politècnica de València, Camino de Vera s/n, 46022 Valencia, Spain

ARTICLE INFO

Keywords:
Internal combustion engine
Variable geometry turbine
Variable valve timing optimization
Turbine inlet temperature

ABSTRACT

Among other advances in spark ignited internal combustion engines' field, the variable geometry turbine (VGT) is being analysed to achieve further CO2 reduction objectives. This paper analyses the potential implications of replacing nowadays standard, the waste-gate (WG) technology, with VGT.

To do so, after developing a robust and validated model, this work proposes a methodology to optimize the variable valve timing (VVT), at full load working conditions, in a new generation spark ignited (SI) engine, coupled to a VGT prototype. The optimization methodology accounts for the different thermo-mechanical limits of such technology compared to the reference WG turbocharger, particularly in terms of the turbine inlet temperature (T3). Torque differences show a systematic improvement by using a VGT, reaching approximately 22 Nm of improvement and about 17 g/kWh, although the difference in torque is smaller after 3500 rpm due to the more restrictive T3 limit imposed.

As well, at partial loads, the same procedure is developed, but targeting the optimization of the engine efficiency. At partial loads, when no exhaust gas recirculation technique is applied, few advantages are identified. However, with exhaust gasses recirculation (EGR) technique, improvements reach 3 g/kWh and permit extending the desired EGR rate towards the lower speeds.

1. Introduction

Internal combustion engine (ICE) upgrades combined with low cost and high-power density fuel availability supported ICE usage over the last decades. However, future limitations on greenhouse gases and other pollutants are expected to become more restrictive, following last year's trends [1,2]. Real Driving Emissions (RDE) regulations are being adopted in the main economic zones worldwide, increasing the interest in engine operation in such realistic situations [3]. Some studies focus on NOx emissions [4] and others on CO2 [5] at real driving conditions. Further pollutant restrictions such as the "zero-emissions" urban areas motivated automotive developers to consider implementing battery electric vehicles (BEV). However, several factors prevent the mass implementation of BEV in the current scenario, including long battery charging time [6], degradation [7] and later recycling issue [8], as well as the raw materials' availability [9] directly impacting the product affordability [10]. What is more, data from Ritchie et al. [11] and BP [12] results in Fig. 1, and reveal that the electricity production would imply charging the BEV using a 61.6% from coal, gas and oil (considering the world electric generation mix).

In this context, engine researchers attempt to improve the ICE at aspects such as cold start [13] and fuel consumption [14]. Consequently, new ideas, such as variable-length intake manifolds [15], low gasoline temperature combustion systems [16] and new engine concepts [17,18] emerge.

Turbocharging the ICE [19] contributes to further reducing CO2 emissions [20]. However, smaller engine architectures require higher boosting for the same performance. Consequently, the turbocharger (TC) operation and its interaction with the rest of the engine hardware becomes a critical point in either transient [21] and steady-state operation [22]. Some examples of nowadays studies regarding turbocharger technology deal with hybrid turbocharging systems [23], new models to represent the turbine and compressor behaviour at extreme operative situations [24] or methodologies to obtain adiabatic turbine maps [25].

Improving TC-ICE matching using VGT technology in gasoline engines has been assessed [26]. This technology was prohibitively expensive for its application in the production of SI ICE, among others, due to the high exhaust temperatures of gasoline engines. This situation has changed with the improvements in materials technology [27,28]. However, still nowadays the VGT implies a more significant restriction at maximum exhaust temperature. To partially solve this, some studies [29] have analysed the impact of using a porous material to enhance the heat transfer phenomena upstream of the turbine. Other

* Corresponding author.
E-mail address: algovi2@mot.upv.es (A. Gómez-Vilanova).

https://doi.org/10.1016/j.applthermaleng.2022.119934
Received 21 June 2022; Received in revised form 15 November 2022; Accepted 20 December 2022
Available online 28 December 2022

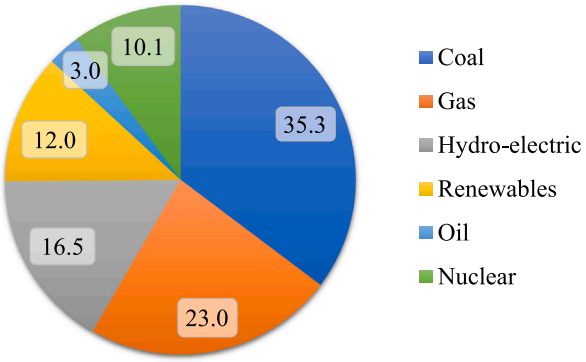

Fig. 1. 2020 world electricity production by source (in %).

studies [30] reveal the potential effects of the water injection strategy on the turbine inlet temperature, stoichiometric operation and spark advance.

Traditionally, in the SI ICE, a mixture enrichment strategy was carried out to protect the turbine from excessive temperatures. However, with new RDE and anti-pollutant regulations, this strategy cannot be longer applied. In this breeding ground, methodologies to reduce the temperature of the exhaust gases include EGR, which simultaneously implies some benefits at partial load and allows for the stoichiometric operation in a larger operative area [31,32]. The usage of EGR technique to improve efficiency [33] and NOx reduction [34] represents another motivation for the VGT implementation. Lujan et al. [34] also evidenced that for gasoline ICE if high EGR rates are pursued, the engine output is highly restricted by the boosting capabilities when implementing a WG turbocharger. Other works show that EGR rates above 40% reduce NOx emissions below 300 ppm, which further backs up the idea of implementing high EGR rates and the requirement of systematic higher boost capabilities [35].

The main scope of this work is the analysis of the impact of the turbocharger thermo-mechanical limitations on the performance of next-generation spark-ignition engines. In particular, this work deals with a new turbocharged SI ICE with VVT. The baseline version of the engine is coupled to a WG turbocharger. However, this study explores the upgrade of the TC system towards the VGT unit and keeping the stoichiometric mixture at any working point, needed for meeting future regulations in terms of unburned hydrocarbons and carbon monoxide emissions management. However, both turbine technologies have different limitation in terms of turbine inlet temperature (T3), particularly 990 °C for the VGT and 1020 °C for the WG for the units under consideration. Therefore, it is necessary to understand the importance of this different limit in the overall engine performance and optimization.

For this purpose, a methodology combining experimental and computational information has been proposed. In a first step, full and partial loads' experimental information is used to develop and validate a 1D engine model for the prospective analysis in this work. Using the model, an optimization of the VVT system is proposed, targeting the maximization of the engine torque at full load at lambda = 1 for each turbocharger technology. The novelty of this optimization lies in the simultaneous maximization of power output, considering all the potential limitations to identify the next generation of engines' potential. This optimization of the VVT is performed while keeping the stoichiometric mixture operation, avoiding fuel enrichment and allowing the use of 3 ways catalysts in the exhaust gases aftertreatment. From a comprehensive perspective, this work analyses and identifies the turbocharger thermo-mechanical limitations restricting engine performance. The primary restrictions potentially impacting the TC-engine performance are determined to be turbine inlet pressure (p3), turbine inlet temperature (T3) and compressor outlet temperature (T2). Particularly from 3000 rpm in advance, the WG performance is limited by the maximum allowed p3, while T3 limits the VGT and engine output. What is more, from the analysis performed, at the high end, working at stoichiometric operation requires diminishing the volumetric efficiency by means of the VVT configuration to protect the turbine. Hence, this work contributes to understanding the potential benefits of replacing the current TC standards in gasoline engines (the WG) with new VGT technology at full loads. The differences are originated from the turbocharger technology and its collateral effects, such as VVT configuration and thermo-mechanical limitations. To the best knowledge of authors, it is the first time is published a work about lambda = 1 full load optimization of SI engines operation with VVT and VGT and respecting 3 ways catalyst operative conditions.

Analogously, the VVT optimization is performed, looking for brake-specific fuel consumption (BSFC) minimization at partial loads. This calculation is performed with and without low-pressure EGR. At throttled conditions, negligible differences emerge. However, with EGR, the engine requires a given value of boosting. In this scenario, the VGT usage, in combination with the EGR technique, leads to improved efficiency and EGR rates compared to the WG.

The benefits of using EGR at partial loads and the expected limitations depending on the TC technology are also evidenced. The assessment also highlights BSFC expected improvement and turbine inlet temperature decrease when implementing EGR in new SI engines.

The interest of this study lies in new SI power-train systems resorting to smaller turbocharged engines that shall work under lambda = 1 configuration while maintaining performance that allows the utilization of vehicles in a wide range of circumstances. All the previous shall be guaranteed while improving the engine efficiency as this work considers.

Table 1
Main engine features.

Type of engine	1.3 L Gasoline Spark-Ignited
Number of cylinders	4
Bore/Stroke	72.2 mm/81.35 mm
Compression ratio	9.6
Maximum engine speed	6200 rpm
Number of valves per cylinder	4 with variable timing
Injection system	Direct injection
Turbocharger	WG (standard) or VGT (upgraded)
Charger cooling	Yes
Pollutant normative	EU6d-Temp

2. Experimental campaign

The SI ICE of this study is one with four cylinders, 1.3 litres (L) of displaced volume, VVT mechanism, direct injection and EU6d-Temp calibration. The original engine version is coupled to a WG turbocharger, while the VGT is analysed in this work for the engine upgraded version. The engine controlling unit (ECU) is calibrated according to the original (or baseline) engine version. In other words, aspects such as the mixture richness control, or VVT configuration are optimized considering the WG turbocharger. Some of the more relevant engine specifications are gathered in Table 1.

A summary of the described variables, the corresponding sensors and their accuracy is included in Table 2. Among others, engine speed, torque, and air and fuel flow rates are registered. Pressure and temperature are recorded at different locations: the test cell environment (0), compressor inlet (1) and outlet (2), intake manifold (2′), turbine inlet (3) and outlet (4). High-resolution pressure sensors for the intake manifold, exhaust manifold and cylinders were also included. High-frequency information samples each 0.5 crank angle degrees according to the encoder using a National Instruments PXI 8233 system.

Two full load series are obtained, one guaranteeing the stoichiometric operation and another in which the ECU regulates the mixture

Table 2
Engine test bench instrumentation.

Variable	Equipment	Range	Accuracy
Speed	Dynamometer tachometer	6000 rpm	0.03% fs
Torque	Dynamometer load cell	±450 N m	0.05% fs
Air flow	AVL Flowsonix air	20 to 720 kg/h	2%
Fuel flow	AVL 733S fuel meter	0–150 kg/h	0.2%
Temperature	K-type thermocouples	−200 to 1250 °C	1.5 °C
Averaged pressure	Kistler Piezo-Resistive Transmitters	0–10 bar	0.2% lin.
High-resolution pressure	AVL ZI33	0 to 250 bar	0.3% lin.

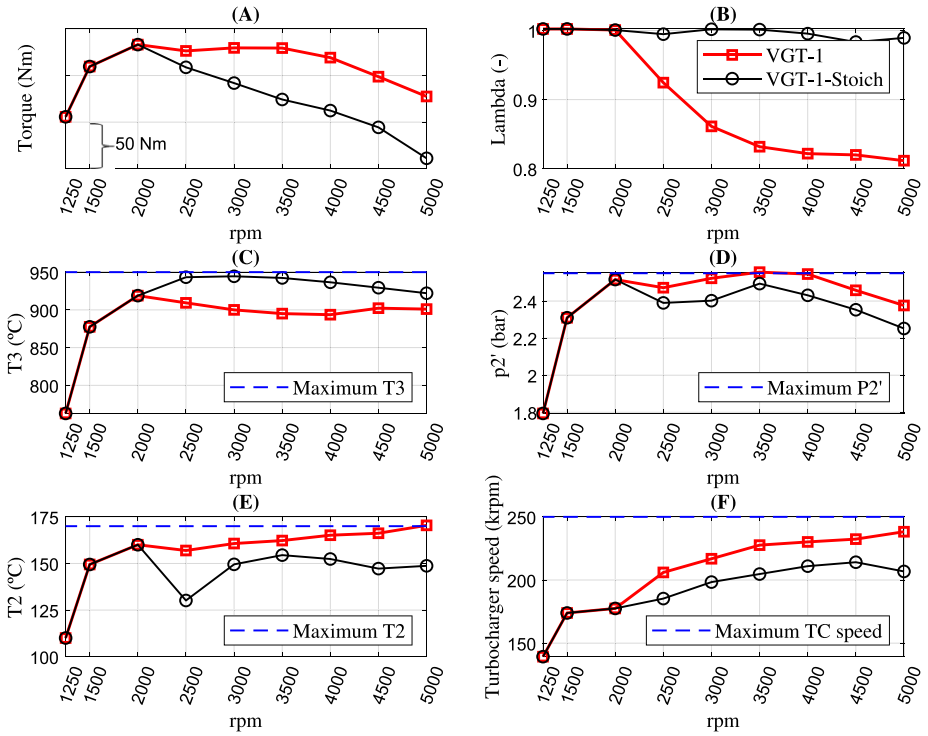

Fig. 2. VGT full load stoichiometric (black) and non-stoichiometric mixture (red) full load experiments. Experimental limitations included (blue).

richness according to the standard engine version calibration. Fig. 2 includes for the VGT the full load results regarding both previously described series. For the stoichiometric series, the engine torque output Fig. 2(A) is restricted by the maximum turbine inlet temperature Fig. 2(C). Accordingly, the only way to avoid surpassing the aforementioned thermo-mechanic limit is through a severe boost pressure level restriction Fig. 2(D). Fig. 2(E) shows compressor outlet temperature, particularly at the high-end torque (5000 rpm) the 170 °C limitation is reached. Finally, Fig. 2(F) evidences the differences in TC speed between both series.

3. Modelling tools

All the experimental information is used for the engine model calibration using GT-Power software for ICE 1D modelling. First, in a first stage, the engine model is fitted and secondly validated.

For the model fitting, an engine calibration procedure adjusts several engine model properties, according to the related experimental data, the most relevant points are the ones that follow:

- First, and just during the fitting, the compressor and turbine are decoupled from each other to limit any uncertainty coming from the turbocharger maps. Consequently, the compressor and turbine become independent elements. On the one hand, the compressor speed is adjusted, looking for an experimental boost pressure. On the other hand, the turbine regulation mechanism (VGT or WG) ensures p3 accomplishment. The throttle regulates the intake manifold pressure (p2′) if needed (i.e. for partial load operation). This technique avoids accounting for the energy balance in the turbocharger. Accordingly, any error/uncertainty during the simulation coming from the turbocharger maps does not impact the rest of the engine operation during the fitting process. The explained technique helps in the models of the engine block fitting, as far as heat transfer [36] and mechanical losses [37] in the turbocharger affect the turbocharger maps, as it has been described the available literature [38]. The effect of such phenomena (mechanical losses or heat transfer) has different impacts as a function of the turbocharger boundaries, leading to potential errors when modelling the TC system in the ICE context. Consequently, some models arise to correct this phenomenon and obtain purely adiabatic maps [38]. This technique is exclusively performed during the fitting. The turbine and compressor are coupled again from the model validation in advance, calling for the quality of the turbocharger maps and considering the TC impact on the engine performance.
- The heat transfer multiplier (HTM) in the elements representing the water charge air cooling is modified to achieve the intake manifold temperature.
- The discrepancies in the pressure drop of the after-treatment between the model and the experiments are corrected using a forward discharge coefficient in the after-treatment line.
- After the simulation converges, any discrepancy in air mass flow is directly attributed to the volumetric efficiency. Hence, the

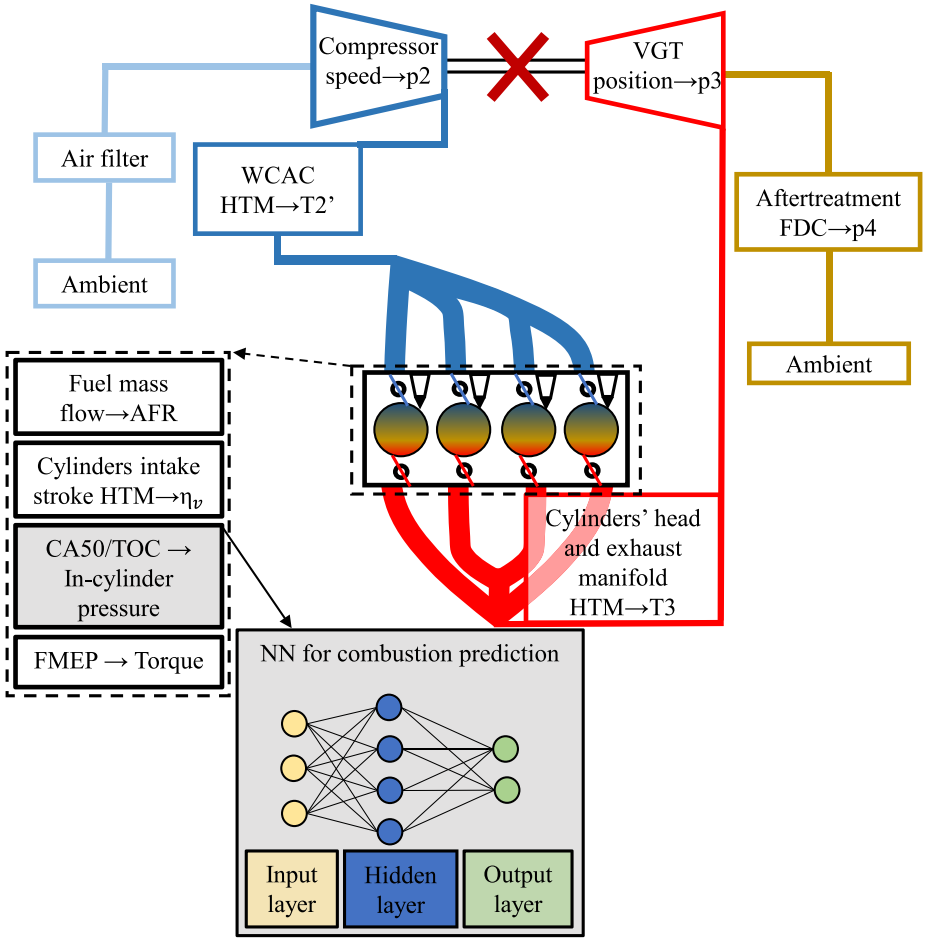

Fig. 3. Schematic of the engine fitting procedure.

cylinders' convection coefficient during the intake stroke is modified to well-predict the experimental fresh air mass flow.

- Wiebe parameters representing the combustion process are adjusted, taking the experimental cylinder pressure evolution as a reference. This procedure modifies the time to achieve 50% (CA50) of the burned mixture as well as the time of combustion (TOC) and the Wiebe parameter (n). Hence, the good combustion prediction results in a good fitting of the experimental cylinder pressure evolution. During this process, in which several combustion parameters are adjusted to follow the experimental pressure traces, a neural network (NN) is trained, taking advantage of the neural network template already built in GT-Power. The obtained combustion parameters (TOC, CA50 and n) correlate to several highly related variables and represent the NN inputs. The selected inputs correspond to engine speed, amount of trapped mass, residuals, temperature and pressure at intake valve closing and AFR. The AFR range during the training considers the stoichiometric composition in the context of full loads, thanks to the specifically dedicated experimental campaign. The NN would be used to predict combustion afterwards being validated.
- For T3 prediction, the exhaust system heat transfer phenomena are adjusted. First, ambient boundaries (cold node) are set up as in the experiments. The same is applied to the cooling water surrounding the exhaust ports. The model computes the heat transfer balance towards/from the exhaust pipes' walls. Accordingly, to fit the experimental heat transfer, turbine inlet temperate is used as the target variable. A proportional–integral–derivative (PID) controller fits the corresponding HTM to reproduce the experimental T3. This HTM is directly applied over the estimated heat transfer coefficient, which follows a Colburn approach. This point is particularly interesting since turbine inlet temperature is one of the main limitations at full loads operative range. According to the engine layout, exhaust ports at the cylinder head are actively cooled in the analysed engine to limit T3.

The obtained coefficients are implemented in the model for later prospective analysis. Fig. 3 provides a schematic diagram of all the previous detailed methodology, including the fitted variables, the TC decoupling as well as the NN development for combustion prediction.

As well, Fig. 4 shows the experimental and model pressure evolution for all three instantaneous signals: cylinder, exhaust manifold and intake manifold. Fig. 4(A) confirms the high degree of matching between experimental and model cylinder pressure, which allows validating the combustion NN performance. Fig. 4(B) and (C) deal with instantaneous exhaust and intake manifold pressures, which, thanks to having considered the complete engine piping during the modelling, can be accurately reproduced. Besides, the high degree of the agreement calls for the model robustness and highly accurate predictions in terms of instantaneous pressure pulse propagation.

Fig. 5 shows the model accuracy when predicting all the main analysed engine variables, including the WG and the VGT. The continuous black series indicate a ±3% experimental to model dispersion. Air mass flow, p2′, torque and p3 are within the desired discrepancy for both series. Regarding turbine temperature, the analysis for the validation considers both: the inlet and outlet. Both Fig. 5(E) for the inlet and Fig. 5(F) for the outlet deal with mass averaged temperature. The model's accuracy in predicting the discussed variables allows for later proposed analysis. Special remarks shall be applied to the accurate

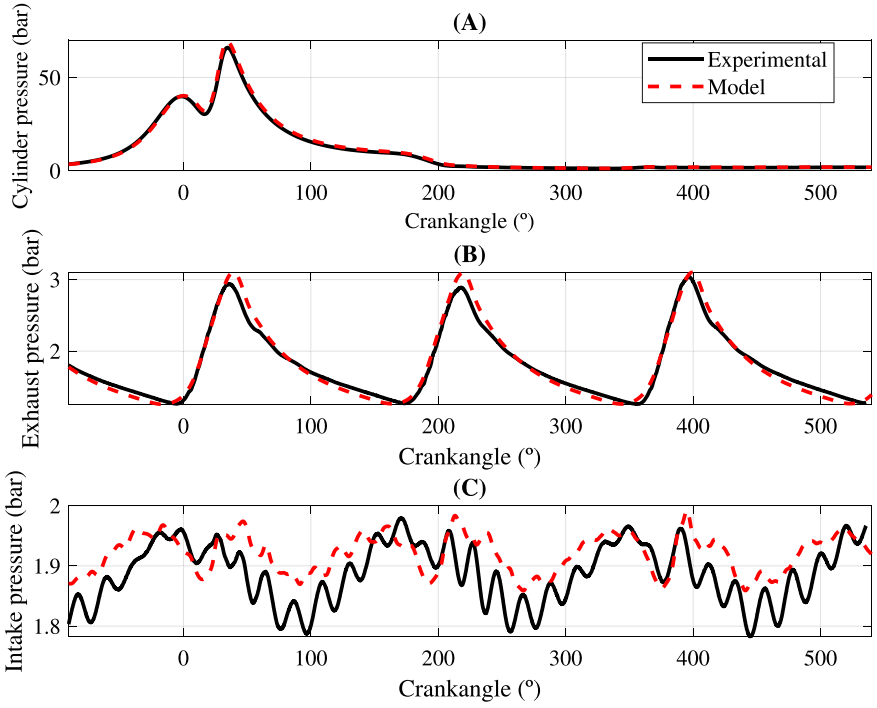

Fig. 4. 1250 rpm full load and VGT instantaneous data validation after the fitting.

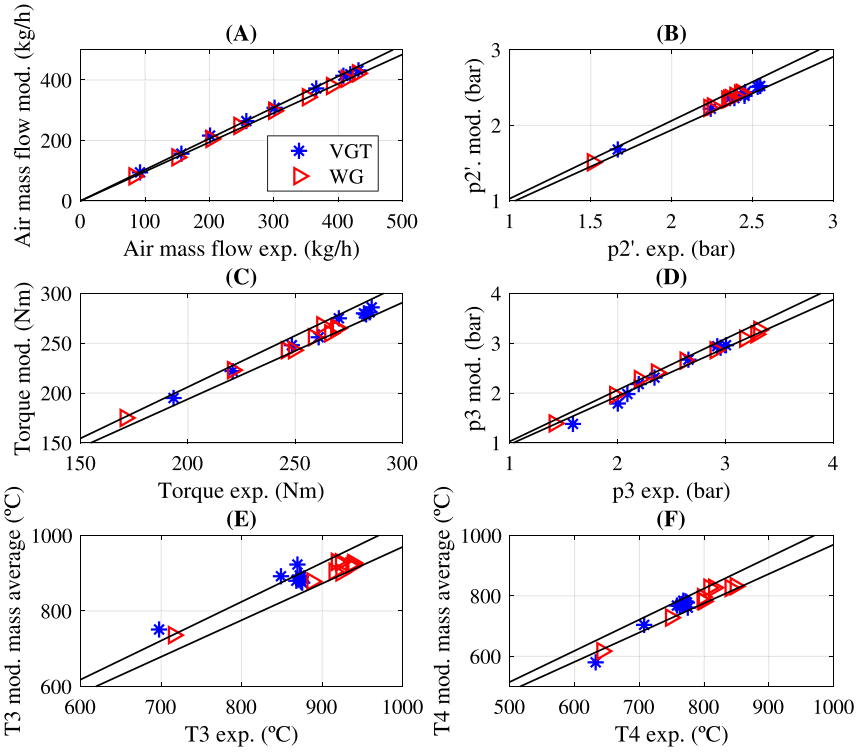

Fig. 5. VGT and WG full load averaged variables validation after the fitting.

prediction regarding turbine inlet pressure and temperature since both would be the primary limiting variables. Hence, a good prediction guarantees a realistic identification of the engine's potential.

4. Optimization methodology

The VVT optimization follows the model validation at full and partial loads. It is assumed that the model accounts for all the crossed relationships and interferences between the several controlling parameters and engine variables. Both intake and exhaust valves setup are varied within the degree of freedom of the actual mechanism, as in Fig. 6 is shown for both extreme positions (maximum and minimum valve overlap).

As previously stated, lambda = 1 conditions are guaranteed, and boost pressure is controlled through the VGT position. Turbine inlet

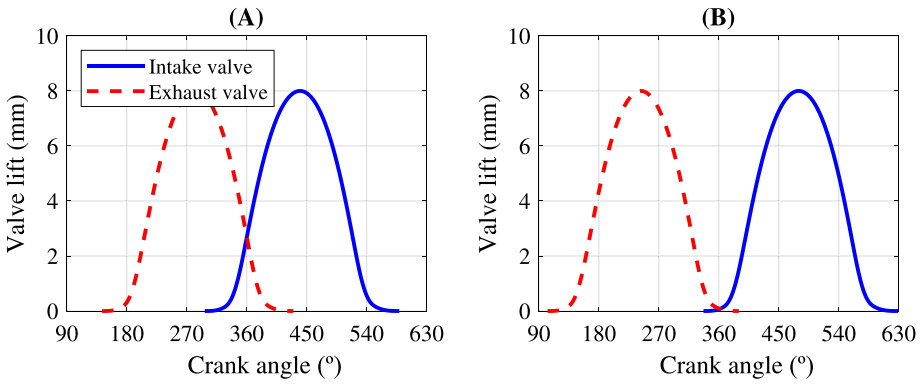

Fig. 6. VVT extreme positions, (A) corresponds to maximum valve overlap and (B) to minimum valve overlap.

Table 3
Turbocharger thermo-mechanical limitations.

Variable	Value
Maximum compressor outlet temperature	170 °C
Maximum boost pressure	2.55 bar
Maximum TC speed	250 krpm
Maximum turbine inlet temperature (WG)	1020 °C
Maximum turbine inlet temperature (VGT)	990 °C
Maximum turbine inlet pressure	3 bar

temperature restriction is also assured through the VGT position controller. If the maximum turbine inlet temperature is overcome, lower boost pressure is pursued, which implies lower air mass flow and a lower amount of injected fuel. The same can be applied to TC speed, p2 and T3, which are controlled by the VGT. Accordingly, if any of the limits mentioned above is surpassed, the VGT position is set up at a more open position pursuing a lower boost, lower TC speed or T2 (whatever is the surpassed limitation). The main limitations are gathered together in Table 3.

A simulation is performed for each VVT combination during the optimization. Consequently, under each evaluated VVT configuration, the maximum engine potential is achieved by reaching at least one thermo-mechanical limitation for each analysed engine point. Depending on the VVT configuration, one different restriction may be achieved sooner or later, leading to different values of engine output. After computing all the possible configurations, it would be possible to choose the optimum solution for each engine speed and the potential benefit compared to the standard calibration. The same procedure has been applied for the partial loads' VVT configuration but looking for BSFC optimization.

Apart from the limits specified in Table 3, the engine trapping ratio "TR" shall be kept above the value of 97% to guarantee proper operation of the 3-ways catalyst. "TR" is defined in Eq. (1), as the ratio between the retained fresh air "$\sum_{i=1}^{n-cylinder} m_{retained}$" and the total amount of fresh air going through the engine "$\int \dot{m}_{inlet}$".

$$TR = \frac{\sum_{i=1}^{n-cylinder} m_{retained}}{\sum_{i=1}^{n-cylinder} \int \dot{m}_{inlet}} \quad (1)$$

4.1. Full loads VVT optimization methodology

Following the methodology, particularly for the VGT and full load operation, the optimization is applied, taking advantage of the validated 1-D engine model.

1250 rpm results for the VVT optimization technique are depicted in Fig. 7, showing the resulting torque and TR. The x-axis corresponds to the intake valve opening (IVO), and the y-axis to the exhaust valve closing (EVC). An EVC of 0° implies that valve closure occurs at the top dead centre (TDC). The same is applied to the IVO. Some valve overlap happens if the IVO is configured before the TDC and the EVC afterwards.

In Fig. 7 the information from the model has been arranged into iso-torque and iso-trapping efficiency areas. After examining the possible configurations, the model can find the areas in which the maximum engine torque output (the objective variable to be optimized). The red asterisks correspond to the ECU calibration, configured according to the WG unit.

It is evidenced how the ECU calibration agrees with the models' optimum solution in terms of torque. However, in terms of TR, a value of around 94.5% is predicted, which is not in the desired range. Furthermore, the model provides valuable information: by just advancing the EVC a few degrees (−5° in this case), torque is kept while TR is improved to the desired 97%. The reason why using the baseline calibration provides an undesired TR output is the one that follows: The VVT calibration was configured for a WG turbocharger, which, for the boost pressure-demand, required a higher value for the turbine inlet pressure, which impedes the short-circuit in a higher degree than the VGT does.

Fig. 8 shows the same information but for 2000 rpm. See how for the 2000 rpm, there is some torque improving margin by just retarding the EVC (increasing the valve overlap). The last is justified by the higher p2′/p3 ratios resulting from the VGT (compared to the WG). Hence, retarding the EVC improves the air mass flow from 224.5 to 229.4 kg/h. In terms of torque benefit, it was improved from 288 N m to 303 N m. Fig. 8 shows the required VVT modification (from the red asterisk to the black circle) for the maximum possible torque while keeping the TR within the desired range.

Detailed results examination to explain the torque improvement reveals how the burnt residuals are reduced from 2.6 to 1.1% of the overall composition inside the cylinder. The in-cylinder composition differences lead to combustion discrepancies: comparing the instantaneous evolution of the cylinder pressure between the ECU set-up and the optimized series, it is obtained Fig. 9, where the less delayed combustion, and corresponding pressure benefit during the expansion stroke is evidenced. This improvement happens thanks to a few CA degrees of spark ignition advance (favouring the optimized series).

Summarizing, the torque increase at 2000 rpm is motivated by the increased air mass flow rate and the slightly more advanced combustion, which enhances engine expansion stroke.

Fig. 10 shows how during the valve overlap period (between 150 and 200 cad), still p2′/p3>1 is guaranteed during most of the time. The last is of high importance from the volumetric efficiency and combustion residuals scavenging perspective. Since VGT presents higher p2/p3 ratio values than the WG does, it is identified that some extra valve overlap improves cylinders scavenging whilst keeping trapping efficiency over the 97% threshold, when moving from WG to VGT technology.

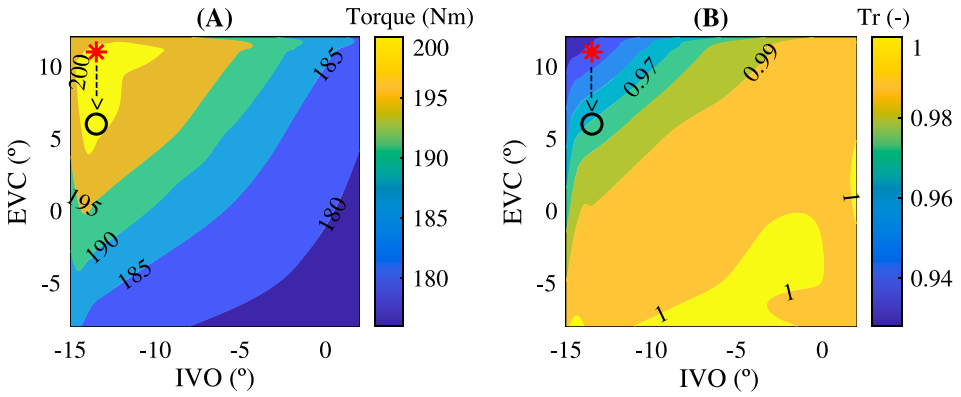

Fig. 7. 1250 rpm VVT model torque optimization results including TR. Asterisk corresponds to ECU calibration and circle to identified optimum.

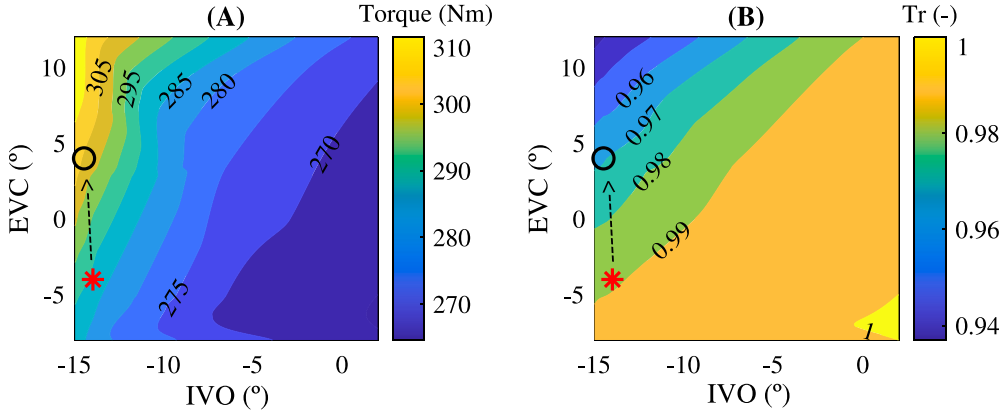

Fig. 8. 2000 rpm VVT model torque optimization results including TR. Asterisk corresponds to ECU calibration and circle to identified optimum.

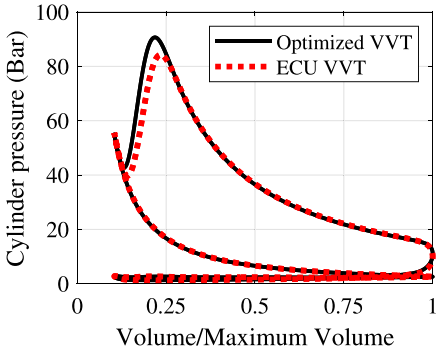

Fig. 9. 2000 rpm, Original and Optimized P-V diagrams.

Finally, to show the consistency of the methodology, Fig. 11(A) shows the torque optimization results for the 5000 rpm case. In contrast, Fig. 11(B) shows turbine inlet temperature for each VVT set-up. TR contours are not included for 5000 rpms since their variation is insensitive regardless of the camshaft configuration with a value >0.99. The high value for the TR is motivated by the fact that the exhaust manifold pressure overcomes the boost value. This situation occurs from 4000 rpm in advance. However, at 5000 rpm, not all the VVT configurations accomplished for T3 limitation, even if the VGT position is at 100% opening, pursuing a lower boost. Indeed, looking at the camshaft configuration following the ECU calibration (red asterisk) results in a value of about 1033 °C. This is the reason why in Fig. 2(B) in the experimental campaign required a given value of mixture richness at the low-end.

During the optimization procedure, it was purposely configured T3 limit as a parameter of design. As a result, the selected configuration (black circle) is chosen since it corresponds to the only one accomplishing T3 restrictions. Torque improvement compared to the standard ECU configuration is very subtle (1.4 N m). In terms of VVT configuration, the difference between the optimum and the ECU configuration relies on advancing the IVO and the EVC by 11 CAD and 9 CAD respectively. This advance diminishes the volumetric efficiency, increasing residual (internal EGR) and reducing the averaged fresh air mass flow from 413 to 391 kg/h. The air mass flow reduction coupled with an almost constant value of one for the TR leads to a lower value of trapped mass in the combustion chamber. The previous provokes a noticeable difference in the cylinder pressure evolution during the compression and expansion stroke, see Fig. 12(A). Subsequently, this pressure decrease allows for a six CAD of advance in the spark plug set-up, contributing to extra advancement in the combustion process and lowering the temperature evolution during the combustion–expansion stroke. Fig. 12(B) evidences this effect for temperature and Fig. 12(C) for the apparent heat release law. The lower gas temperature during the exhaust stroke directly impacts T3 as in Fig. 12(D) is evidenced, including the four pulses (one coming from each cylinder). The dashed series correspond to the mass averaged values for the turbine inlet temperature.

At high-end torque, if the stoichiometric operation is pursued, the VVT has to be set up in a configuration that diminishes the volumetric efficiency to protect the turbine inlet from excessive temperatures. As a collateral effect, the combustion phasing can be slightly advanced, further protecting the turbine. Here, the cross-relationship between the different engine actuators and thermo-mechanical limits is evidenced, focusing on new VGT prototypes.

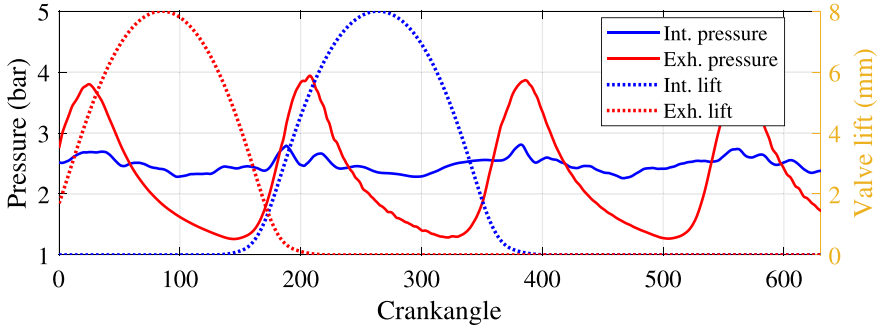

Fig. 10. 2000 rpm, intake manifold and exhaust manifold pressure as well as intake and exhaust valve lifts after applying the VVT optimization in the VGT configuration.

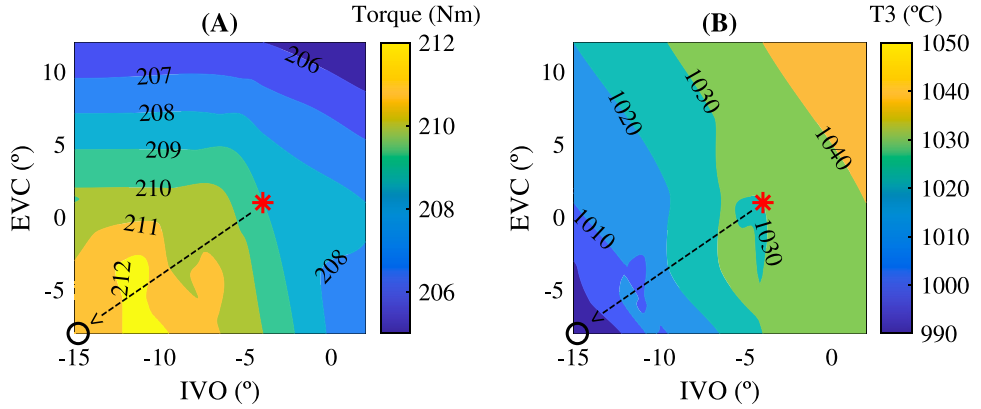

Fig. 11. 5000 rpm VVT model torque optimization results and resulting T3. Asterisk corresponds to ECU calibration and circle to identified optimum.

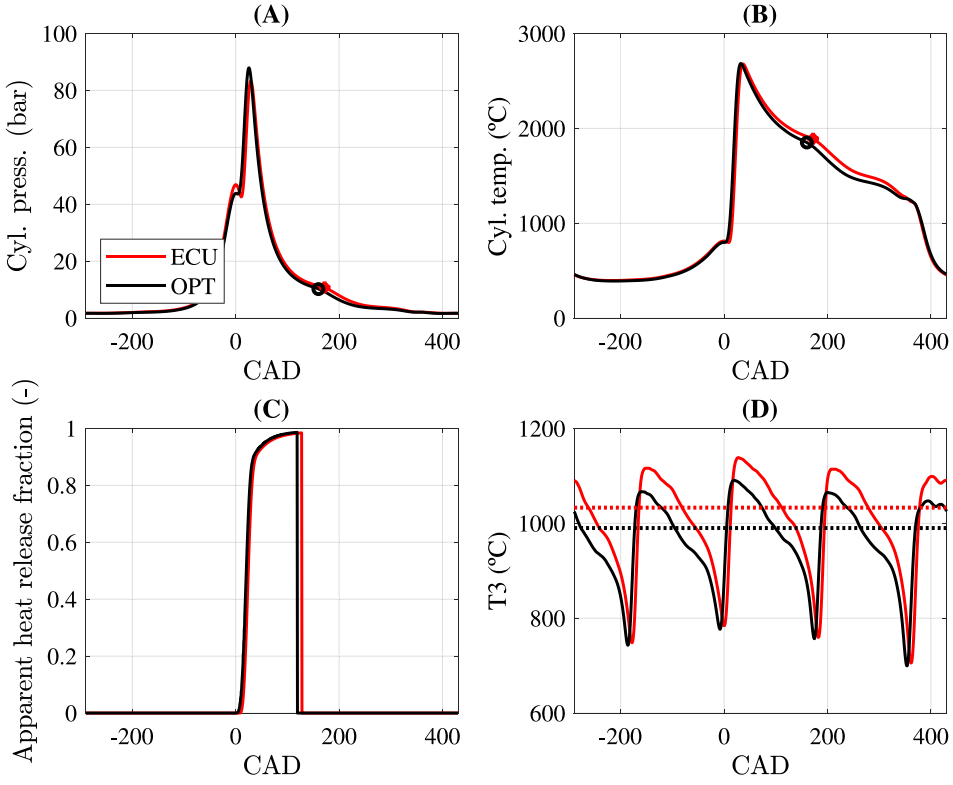

Fig. 12. 5000 rpm analysis for the VVT modification and improvements in turbine inlet temperature. Symbols call for exhaust valve opening.

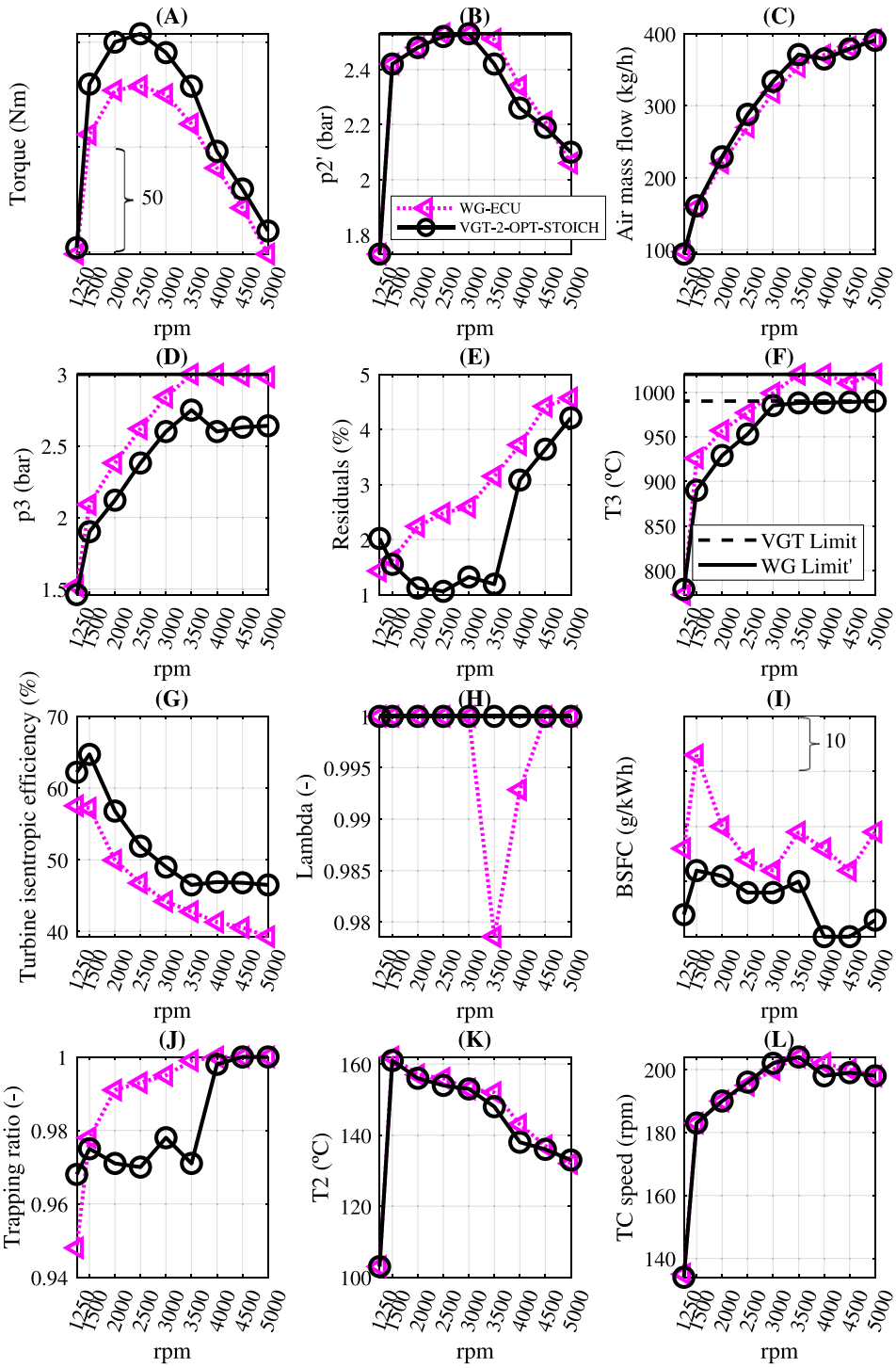

Fig. 13. Full loads including: WG with VVT management governed by ECU calibration and VGT with VVT optimized according to maximum engine power criteria and stoichiometric mixture.

5. Results

5.1. Full loads

Fig. 13 shows the complete engine full load curve (from 1250 to 5000 rpm) for both series of data:

- "VGT-OPT-STOICH" labelled series corresponds to the obtained full load series after optimizing the VVT according to the previously discussed methodology (black circles). The engine is coupled to a VGT turbine and the mixture is kept stoichiometric in any case. The temperature limitation is 990 °C.
- "WG-ECU" series corresponds to the engine baseline configuration: the engine block is coupled to a WG turbocharger (magenta

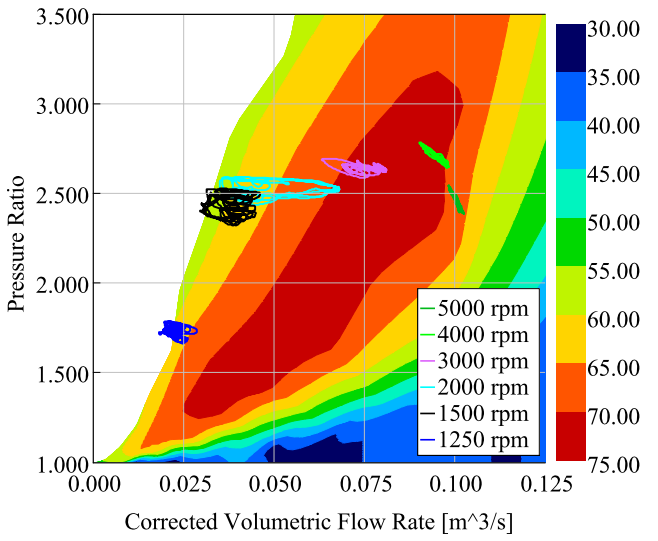

Fig. 14. Compressor efficiency map with several engine working points for the VGT TC.

triangles). The VVT configuration selected is the one from the ECU, which was optimized considering the WG turbocharger. In this series, when required, some mixture enrichment is applied by the AFR controller despite drawbacks in emissions/consumption to protect the turbine side from excessive temperatures, which shall not overcome the barrier of 1020 °C.

Fig. 13(A), which deals with torque information, evidences the VGT-OPT-STOICH higher output, especially from 1250–3000 rpm. In this range, the boost pressure level is the same for both series; see Fig. 13(B). Accordingly, the torque differences come from the combination of other aspects. First, the higher air mass flow Fig. 13(C) thanks to the volumetric efficiency enhancement in the VGT-OPT-STOICH series. The volumetric efficiency improvement is originated by the lower p3 Fig. 13(D) and the VVT optimization. The motivation for the higher torque in the 1250–3000 rpm, despite the same boost, also lies in the residuals' mass fraction differences, see Fig. 13(E). As previously analysed, in Fig. 9 for the 2000 rpm, diminishing the residuals allows for some extra spark and combustion timing advance.

From 1250 to 2000 rpm, boost pressure is limited by compressor surge, as shown in Fig. 14 dealing with the compressor map. Blue, red and cyan series included in Fig. 14 correspond to the operative area in the compressor map for 1250, 1500 and 2000 rpm respectively (VGT-OPT-STOICH). As a matter of fact, the 3000, 4000 and 5000 rpm have been included to show their corresponding operative area. In the speed range between 2500 and 3000 rpm, the boost pressure is the main thermo-mechanical limitation for both data series.

Torque differences in the range of 3500–5000 rpm are lower but slightly favourable to the VGT-OPT-STOICH. Despite the lower boost in the VGT-OPT-STOICH series, the lower p3 and the VVT optimization (with all the implications in combustion and T3) compensate for this effect. In this range (3500–5000 rpm), each series of data presents one limitation preventing the maximum boost pressure from being achieved (limiting torque in consequence). On the one hand, in the VGT series, the limitation is T3, as shown in Fig. 13(F); two aspects contribute to this: the lower affordable T3 and the imposed lambda = 1 operation. On the other hand, the WG series limitation is p3; this is a symptom of lower turbine efficiency Fig. 13(G). Furthermore, for the WG series, only at 3500 and 4000 rpm some mixture enrichment is required to protect the turbine from excessive temperatures, see Fig. 13(H).

Apart from the torque differences, BSFC figures are systematically improved by 2–20 g/kWh depending on the working point, as Fig. 13(I) shows. Several phenomena contribute to this; first, the lower turbine inlet pressure is directly related to lower pumping losses. Secondly but with a more important effect, as previously analysed, VVT setup and its impact on residuals allow for further advance regarding spark phasing, leading to a more efficient combustion process.

Table 4
BSFC improvement after VVT optimization for the 12 BMEP working points.

rpm	4000	3000	2500	2000
BSFC difference (%)	−0.195	−0.130	−0.079	−0.157

All the previously stated was achieved while guaranteeing the TR>0.97 along with the complete engine operation Fig. 13(J). TC speed and maximum compressor outlet temperature limitation are not reached in any case; see Fig. 13(K) and (L).

This comparison aims to detect and evidence the potential benefit by taking profit of the synergies between VGT and VVT optimization while guaranteeing a stoichiometric mixture, which is positive for the after-treatment efficiency, the BSFC and pollutant emissions. The VVT optimization in such scenario is required for the following:

- Increasing the trapped ratio in the low-end.
- Improving the volumetric efficiency and reducing the residuals in the middle range. This also contributes to a more favourable combustion phasing.
- Limiting T3 to guarantee the safe turbine operation when VGT is fully open in the high-end. This is even more relevant to compensate for VGT's lower T3 limit (in comparison to WG).

5.2. Partial loads (12 bar BMEP)

Here, the VVT analysis targets the BSFC optimization at partial load operation. 12 bar of BMEP and a speed range from 2000 to 4000 rpm were evaluated and correspond to the operative area where the VGT mechanism is entirely open. Consequently, the throttle body regulates the desired boost pressure. T3 and the rest of the engine thermo-mechanic limitations are far from being reached.

It was not identified any BSFC improvement for the throttled operative range. Eq. (2) is used for the BSFC difference calculation in relative terms after the optimization procedure. Sub-index "i" in Eq. (2) corresponds to each evaluated engine speed. Results are included in Table 4, and differences do not reach the 0.2% improvement when comparing the optimized VVT results versus those with the ECU baseline VVT strategy (the one coming from WG configuration).

$$Difference = \frac{BSFC_i^{VGT-OPT} - BSFC_i^{VGT-ECU}}{BSFC_i^{VGT-ECU}} * 100 \quad (2)$$

EGR usage for efficiency improvement at partial loads is a novel technique [34] whose impact has been considered in this section. The simulations were configured to achieve a 27% of low-pressure EGR simultaneously to a BMEP of 12 bar. In the previously described studies (partial loads without EGR), the engine was partially throttled to achieve the 12 bar BMEP demand. However, for the same load, under 27% of EGR, the throttle body remains completely open, and some boost is required to achieve the desired engine output. Hence, in this part of the study, the required boost for the load demand is controlled through the WG or VGT actuation. The EGR is controlled through an EGR valve, connecting a section downstream of the after-treatment with a section upstream compressor inlet. Results are included in Fig. 15, where empty series are the points with EGR and bold series those without EGR.

Fig. 15(A) shows the predicted BSFC regarding both series for each TC: with and without EGR. First, comparing the series with and without EGR shows the expected differences. The lower averaged cylinder temperature (reducing heat losses) and the possibility of optimizing the combustion process, leads to a more efficient operation when EGR is

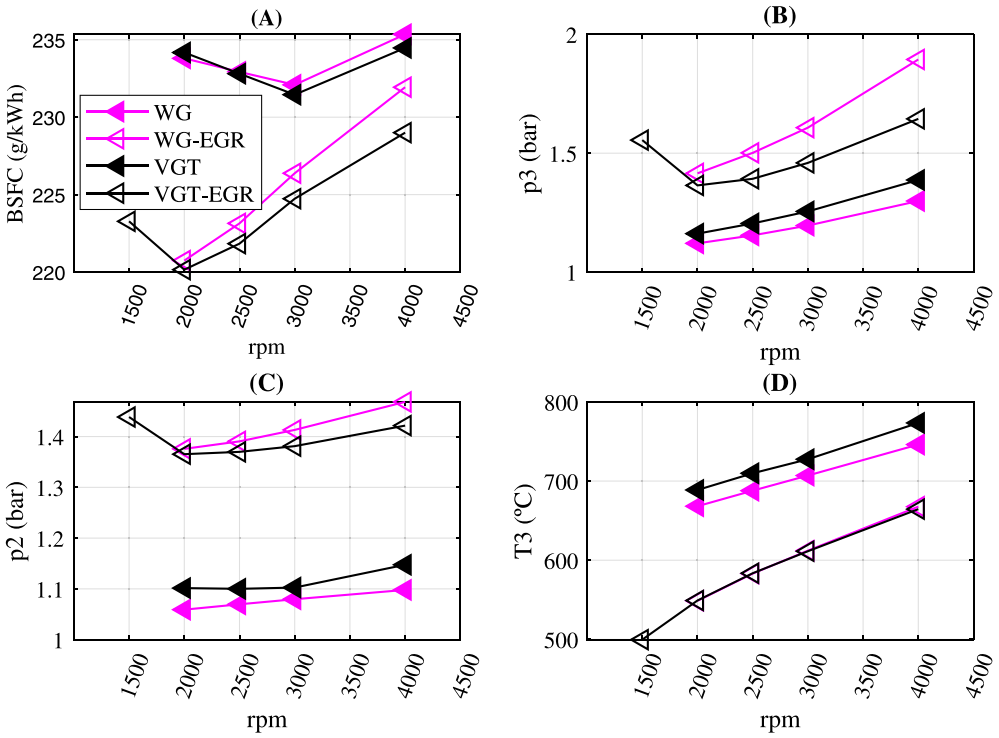

Fig. 15. 12 bar BMEP points for both turbocharger units, with and without EGR.

used, aligned with results in [33,34]. As well, comparing the series with and without EGR show how the engine works under boosted operation (not throttled). The boost requirements increase in the order of 0.3 bar approximately when EGR is used, see Fig. 15(C).

Furthermore, comparing WG vs VGT series, both under EGR configuration, shows potential improvements up to 3 g/kWh in the 4000 rpm point. The VGT series can also extend the EGR technique (up to 27% EGR) towards 1500 rpm, which is not possible for the WG series, reaching the maximum WG closure (and boost limitation). BSFC differences between VGT and WG series (with EGR) are mainly motivated by p3 discrepancies, see Fig. 15(B). The WG series exhaust manifold pressure is systematically higher, overcoming the VGT series by 0.23 bar at 4000 rpm, this is motivated by the VGT higher efficiency. Boost pressure is included in Fig. 15(C), showing differences in the intake manifold requirements to achieve the same BMEP. A higher boost pressure is required in the WG series to compensate for the higher p3 accordingly.

Finally, Fig. 15(D) evidences the turbine inlet temperature decrease after using EGR. An offset of about 80 °C is achieved systematically, with lower temperatures when EGR is used. Which may represent a collateral benefit from the thermal fatigue perspective [39].

In all, the VGT could extend the EGR target of 27% towards lower engine speeds, which was not possible in the WG turbocharger due to the lack of boost to compensate for the higher boost requirements. BSFC differences between turbine technologies increase with EGR employment since higher boost levels are targeted, and the resulting p3 differences impact the engine efficiency.

6. Conclusions

This work uses the developed model to evaluate the potential benefits of collecting the synergies between stoichiometric operation and VGT technology usage during a VVT optimization procedure. In a first step, an extensive experimental campaign to correlate a robust 1-D model of a new SI ICE. The model calibration includes all the potential uncertainties and highly impacting phenomena, such as combustion and heat transfer effects at the exhaust line at both high and low pressure ends. Then, the calibrated model is used to identify the VVT configuration depending on the target: maximum engine output (identifying full load curve) or maximum efficiency (at partial load points), guaranteeing that any thermo-mechanical limitation is overcome and that the trapping efficiency is high enough to keep the maximum efficiency of 3-ways catalyst after-treatment.

After the optimization, this work describes in detail the mechanisms that justify the expected improvements between the baseline version of the analysed engine (coupled to a WG) and the upgraded version (coupled to a VGT and operating at lambda = 1). As well this work identifies the limiting parameters:

- On the one hand, at full loads, the upgraded version of the engine shows consistent improvements in terms of torque. Depending on the engine speed, improvements are expected to rise up to 22 N m, while some benefit is obtained through the complete engine range. The full load curve in the VGT series also shows a consistent efficiency improvement, reducing the BSFC up to 17 g/kWh. The turbocharger technology originates the observed engine output differences. From 1250–3000 rpm, for the same boost pressure, the WG turbocharger requires higher values of p3. The higher engine back pressure has some collateral effects regarding air mass flow, cylinder composition and combustion phasing. Therefore, p3 reduction leads to improved performance in the VGT. From 3000 rpm in advance, while turbine inlet pressure is the limitation for the WG, this limitation is never reached in the case of the VGT. The turbine inlet temperature is the limitation of the VGT in the high-end. However, the results section reveals that even though the lower allowed T3 in the VGT, a systematic improvement regarding torque and BSFC is expected. In the low end, the VVT is optimized, looking for improvements in the trapping ratio. At the middle-speed range, the VVT pursues to improve the volumetric efficiency and the composition of the trapped mixture leading to improvements in the engine output. Finally, to protect the turbine at the high end, the VVT has to deteriorate the volumetric efficiency, with collateral effects on combustion and T3.

- On the other hand, no advantage was identified at part loads due to throttled operation when no EGR is employed. However, with EGR, the VGT implies an improvement up to 3 g/kWh with respect to the WG. Furthermore, the minimum engine speed at which the VGT can keep the desired engine load for the 27% EGR rate is reduced up to 1500 rpm. For the WG, the minimum speed was 2000 rpm, limited by the WG closure. Finally, comparing the calculations with and without EGR shows a turbine inlet temperature reduction of approximately 80 °C. BSFC can be improved up to 14 g/kWh at 2000 rpm and 6 g/kWh at 4000 rpm, comparing the VGT study with versus without EGR.

Declaration of competing interest

The authors declare that they have no known competing financial interests or personal relationships that could have appeared to influence the work reported in this paper.

Data availability

The data that has been used is confidential.

Acknowledgements

This research has been supported by Grant PID2020-114289RB-I00 funded by MCIN/AEI/10.13039/501100011033. The authors wish to thank Vicente Esteve Ferrer for his invaluable work during the experimental campaign.

References

[1] E. Massaguer, A. Massaguer, T. Pujol, M. Comamala, L. Montoro, J.R. Gonzalez, Fuel economy analysis under a WLTP cycle on a mid-size vehicle equipped with a thermoelectric energy recovery system, Energy 179 (2019) 306–314, http://dx.doi.org/10.1016/j.energy.2019.05.004.

[2] J. Pavlovic, B. Ciuffo, G. Fontaras, V. Valverde, A. Marotta, How much difference in type-approval CO2 emissions from passenger cars in europe can be expected from changing to the new test procedure (NEDC vs. WLTP)? Transp. Res. A 111 (October 2017) (2018) 136–147, http://dx.doi.org/10.1016/j.tra.2018.02.002.

[3] U. Tietge, P. Mock, V. Franco, N. Zacharof, From laboratory to road: Modeling the divergence between official and real-world fuel consumption and CO2 emission values in the german passenger car market for the years 2001–2014, Energy Policy 103 (January) (2017) 212–222, http://dx.doi.org/10.1016/j.enpol.2017.01.021.

[4] R. Suarez-Bertoa, P. Mendoza-Villafuerte, F. Riccobono, M. Vojtisek, M. Pechout, A. Perujo, C. Astorga, On-road measurement of NH3 emissions from gasoline and diesel passenger cars during real world driving conditions, Atmos. Environ. 166 (2017) 488–497, http://dx.doi.org/10.1016/j.atmosenv.2017.07.056.

[5] G. Fontaras, N.G. Zacharof, B. Ciuffo, Fuel consumption and CO2 emissions from passenger cars in Europe – laboratory versus real-world emissions, Prog. Energy Combust. Sci. 60 (2017) 97–131, http://dx.doi.org/10.1016/j.pecs.2016.12.004.

[6] M. Neaimeh, S.D. Salisbury, G.A. Hill, P.T. Blythe, D.R. Scoffield, J.E. Francfort, Analysing the usage and evidencing the importance of fast chargers for the adoption of battery electric vehicles, Energy Policy 108 (June) (2017) 474–486, http://dx.doi.org/10.1016/j.enpol.2017.06.033.

[7] J. Du, X. Zhang, T. Wang, Z. Song, X. Yang, H. Wang, M. Ouyang, X. Wu, Battery degradation minimization oriented energy management strategy for plug-in hybrid electric bus with multi-energy storage system, Energy 165 (2018) 153–163, http://dx.doi.org/10.1016/j.energy.2018.09.084.

[8] J.P. Skeete, P. Wells, X. Dong, O. Heidrich, G. Harper, Beyond the event horizon: Battery waste, recycling, and sustainability in the United Kingdom electric vehicle transition, Energy Res. Soc. Sci. 69 (April) (2020) 101581, http://dx.doi.org/10.1016/j.erss.2020.101581.

[9] B. Jones, R.J. Elliott, V. Nguyen-Tien, The EV revolution: The road ahead for critical raw materials demand, Appl. Energy 280 (October) (2020) 115072, http://dx.doi.org/10.1016/j.apenergy.2020.115072.

[10] J. Zhao, X. Xi, Q. Na, S. Wang, S.N. Kadry, P.M. Kumar, The technological innovation of hybrid and plug-in electric vehicles for environment carbon pollution control, Environ. Impact Assess. Rev. 86 (September 2020) (2021) http://dx.doi.org/10.1016/j.eiar.2020.106506.

[11] H. Ritchie, M. Roser, CO and greenhouse gas emissions, Our World Dat (2020) URL https://ourworldindata.org/co2-and-other-greenhouse-gas-emissions.

[12] B.S. Review, Statistical Review of World Energy, Tech. Rep., BP, 2020, pp. 1–56, URL bp.com/statisticalreview.

[13] A. Zare, T.A. Bodisco, M. Jafari, P. Verma, L. Yang, M. Babaie, M.M. Rahman, A. Banks, Z.D. Ristovski, R.J. Brown, S. Stevanovic, Cold-start NOx emissions: Diesel and waste lubricating oil as a fuel additive, Fuel 286 (P2) (2021) 119430, http://dx.doi.org/10.1016/j.fuel.2020.119430.

[14] J. Pavlovic, G. Fontaras, S. Broekaert, B. Ciuffo, M.A. Ktistakis, T. Grigoratos, How accurately can we measure vehicle fuel consumption in real world operation? Transp. Res. D 90 (December 2020) (2021) 102666, http://dx.doi.org/10.1016/j.trd.2020.102666.

[15] H. Talati, K. Aliakbari, A. Ebrahimi-Moghadam, H. Khoshbakht Farokhad, A. Eskandary Nasrabad, Optimal design and analysis of a novel variable-length intake manifold on a four-cylinder gasoline engine, Appl. Therm. Eng. 200 (April 2021) (2022) 117631, http://dx.doi.org/10.1016/j.applthermaleng.2021.117631.

[16] H. Yun, C. Idicheria, P. Najt, The effect of advanced ignition system on gasoline low temperature combustion, Int. J. Engine Res. 22 (2) (2021) 417–429, http://dx.doi.org/10.1177/1468087419867543.

[17] J.R. Serrano, F.J. Arnau, P. Bares, A. Gomez-Vilanova, J. Garrido-Requena, M.J. Luna-Blanca, F.J. Contreras-Anguita, Analysis of a novel concept of 2-stroke rod-less opposed pistons engine (2S-ROPE): Testing, modelling, and forward potential, Appl. Energy 282 (PA) (2021) 116135, http://dx.doi.org/10.1016/j.apenergy.2020.116135.

[18] Y. Zhou, A. Sofianopoulos, B. Lawler, S. Mamalis, Advanced combustion free-piston engines: A comprehensive review, Int. J. Engine Res. 21 (7) (2020) 1205–1230, http://dx.doi.org/10.1177/1468087418800612.

[19] H. Hiereth, P. Prenninger, Charging the Internal Combustion Engine, Springer, Vienna, 2007, pp. 1–268, http://dx.doi.org/10.1007/978-3-211-47113-5.

[20] A.J. Feneley, A. Pesiridis, A.M. Andwari, Variable geometry turbocharger technologies for exhaust energy recovery and boosting-A review, Renew. Sustain. Energy Rev. 71 (September 2015) (2017) 959–975, http://dx.doi.org/10.1016/j.rser.2016.12.125.

[21] Y. Park, I. Park, K. Min, M. Sunwoo, Model-based feedforward control of the VGT in a diesel engine based on empirical models of compressor and turbine efficiencies, Int. J. Automot. Technol. 16 (4) (2015) 561–570, http://dx.doi.org/10.1007/s12239-015-0057-7, URL http://link.springer.com/article/10.1007/s12239-012-0027-2.

[22] M. Wöhr, E. Chebli, M. Müller, H. Zellbeck, J. Leweux, A. Gorbach, Development of a turbocharger compressor with variable geometry for heavy-duty engines, Int. J. Engine Res. (ISSN: 20413149) 16 (1) (2015) 23–30, http://dx.doi.org/10.1177/1468087414562457.

[23] Q. Zhou, Z. Yin, H. Zhang, T. Wang, W. Sun, C. Tan, Performance analysis and optimized control strategy for a three-shaft, recuperated gas turbine with power turbine variable area nozzle, Appl. Therm. Eng. (ISSN: 13594311) 164 (July 2019) (2020) 114353, http://dx.doi.org/10.1016/j.applthermaleng.2019.114353, URL https://doi.org/10.1016/j.applthermaleng.2019.114353.

[24] A. Tiseira, L.M. García-Cuevas, L.B. Inhestern, J.D. Echavarría, Development of choked flow in variable nozzle radial turbines, Int. J. Engine Res. (2021) http://dx.doi.org/10.1177/14680874211018302.

[25] J.R. Serrano, F.J. Arnau, L.M. Garcı á Cuevas, A. Gómez-Vilanova, S. Guilain, S. Batard, A methodology for measuring turbocharger adiabatic maps in a gas-stand and its usage for calibrating control oriented and one-dimensional models at early ICE design stages, J. Energy Resour. Technol. Trans. ASME 143 (4) (2021) 1–12, http://dx.doi.org/10.1115/1.4048229.

[26] J.R. Serrano, P. Piqueras, J. De la Morena, A. Gómez-Vilanova, S. Guilain, Methodological analysis of variable geometry turbine technology impact on the performance of highly downsized spark-ignition engines, Energy 215 (2021) http://dx.doi.org/10.1016/j.energy.2020.119122.

[27] V.O. Shettigar, A. Pesiridis, Materials selection for variable geometry turbine nozzle for gasoline engine application, in: Proceedings of the ASME Turbo Expo, Vol. 1B, 2014, pp. 1–11, http://dx.doi.org/10.1115/GT2014-27119.

[28] S. Jung, Y.H. Jo, C. Jeon, W.M. Choi, B.J. Lee, Y.J. Oh, G.Y. Kim, S. Jang, S. Lee, Effects of mn and mo addition on high-temperature tensile properties in high-Ni-containing austenitic cast steels used for turbo-charger application, Mater. Sci. Eng. A 682 (September 2016) (2017) 147–155, http://dx.doi.org/10.1016/j.msea.2016.11.006.

[29] D. Dong, Y. Moriyoshi, J. Zhu, To improve the performance of a variable geometry turbocharged SI engine by porous material application, Appl. Therm. Eng. 197 (December 2020) (2021) 117373, http://dx.doi.org/10.1016/j.applthermaleng.2021.117373.

[30] D. Lanni, E. Galloni, G. Fontana, Numerical analysis of the effects of port water injection in a downsized SI engine at partial and full load operation, Appl. Therm. Eng. 205 (January 2021) (2022) 118060, http://dx.doi.org/10.1016/j.applthermaleng.2022.118060.

[31] K. Shen, F. Li, Z. Zhang, Y. Sun, C. Yin, Effects of LP and HP cooled EGR on performance and emissions in turbocharged GDI engine, Appl. Therm. Eng. 125 (x) (2017) 746–755, http://dx.doi.org/10.1016/j.applthermaleng.2017.07.064.

[32] M. Sjerić, I. Taritaš, R. Tomić, M. Blažić, D. Kozarac, Z. Lulić, Efficiency improvement of a spark-ignition engine at full load conditions using exhaust gas recirculation and variable geometry turbocharger – numerical study, Energy Convers. Manage. 125 (2016) 26–39, http://dx.doi.org/10.1016/j.enconman.2016.02.047.

[33] H. Climent, V. Dolz, B. Pla, D. González-Domínguez, Analysis on the potential of EGR strategy to reduce fuel consumption in hybrid powertrains based on advanced gasoline engines under simulated driving cycle conditions, Energy Convers. Manage. 266 (May) (2022) http://dx.doi.org/10.1016/j.enconman.2022.115830.

[34] J.M. Luján, H. Climent, R. Novella, M.E. Rivas-Perea, Influence of a low pressure EGR loop on a gasoline turbocharged direct injection engine, Appl. Therm. Eng. 89 (2015) 432–443, http://dx.doi.org/10.1016/j.applthermaleng.2015.06.039.

[35] C. Jiang, G. Huang, G. Liu, Y. Qian, X. Lu, Optimizing gasoline compression ignition engine performance and emissions: Combined effects of exhaust gas recirculation and fuel octane number, Appl. Therm. Eng. 153 (November 2018) (2019) 669–677, http://dx.doi.org/10.1016/j.applthermaleng.2019.03.054.

[36] J.R. Serrano, P. Olmeda, F.J. Arnau, A. Dombrovsky, L. Smith, Turbocharger heat transfer and mechanical losses influence in predicting engines performance by using one-dimensional simulation codes, Energy 86 (2015) 204–218, http://dx.doi.org/10.1016/j.energy.2015.03.130.

[37] J.R. Serrano, P. Olmeda, A. Tiseira, L.M. García-Cuevas, A. Lefebvre, Importance of mechanical losses modeling in the performance prediction of radial turbochargers under pulsating flow conditions, SAE Int. J. Engines 6 (2) (2013) 729–738, http://dx.doi.org/10.4271/2013-01-0577.

[38] J.R. Serrano, P. Olmeda, F.J. Arnau, V. Samala, A holistic methodology to correct heat transfer and bearing friction losses from hot turbocharger maps in order to obtain adiabatic efficiency of the turbomachinery, Int. J. Engine Res. 21 (8) (2020) 1314–1335, http://dx.doi.org/10.1177/1468087419834194.

[39] M. Bartošák, M. Španiel, K. Doubrava, Thermo-mechanical fatigue of SiMo 4.06 turbocharger turbine housing: Damage operator approach, Eng. Fail. Anal. 105 (March 2018) (2019) 736–755, http://dx.doi.org/10.1016/j.engfailanal.2019.06.068.